This is a preprint draft. The published article can be found at:
http://www.sciencedirect.com/science/article/pii/S0261306914003392

Please cite this paper as:
G. Sakar, R.A. Hawileh, M.Z. Naser, J.A. Abdalla, M. Tanarslan, Nonlinear behavior of shear deficient RC beams strengthened with near surface mounted glass fiber reinforcement under cyclic loading, Materials & Design, Volume 61, September 2014, Pages 16-25, ISSN 0261-3069, https://doi.org/10.1016/j.matdes.2014.04.064.

Nonlinear behavior of shear deficient RC beams strengthened with near surface mounted glass fiber reinforcement under cyclic loading

M. Tanarslan[1], R.A. Hawileh[2], M.Z. Naser[2], J.A. Abdalla[2]

[1] Dokuz Eylul University
Department of Civil Engineering, Buca, Izmir 35160, Turkey, murat.tanarslan@deu.edu.tr

[2] American University of Sharjah
Department of Civil Engineering, P.O. Box 26666, Sharjah, UAE, E-mail: *rhaweeleh@aus.edu,
*Corresponding Author: Rami Hawileh, Ph.D.

ABSTRACT

This paper presents both experimental and 3D nonlinear Finite Element (FE) simulation of shear deficient reinforced concrete (RC) cantilever beams strengthened with Near Surface Mounted (NSM) Glass Fiber Reinforced polymer (GFRP) rods subjected to cyclic loading. A series of five RC beams were tested under cyclic loading up to failure. A three-dimensional Finite Element (FE) model was also developed to simulate the response of the tested specimens. The developed FE model integrates multiple simulation techniques, nonlinear material properties and corresponding constitutive laws. The models incorporate concrete cracking, yielding of steel reinforcement, bond-slip behavior between NSM reinforcement and adhesive material and between steel reinforcement and adjacent concrete material, respectively. The FE models predicted results were compared with the measured experimental results via a comparison of load-deflection response envelopes and load-deflection hysteresis loops. Good matching between the experimental results and FE simulation was observed. The experimental results indicates that the use of GFRP rods as NSM strengthening systems can significantly enhance the overall capacity of shear deficient RC members subjected to cyclic loading. These findings have validated by the FE results.

Please cite this paper as:
G. Sakar, R.A. Hawileh, M.Z. Naser, J.A. Abdalla, M. Tanarslan, Nonlinear behavior of shear deficient RC beams strengthened with near surface mounted glass fiber reinforcement under cyclic loading, Materials & Design, Volume 61, September 2014, Pages 16-25, ISSN 0261-3069, https://doi.org/10.1016/j.matdes.2014.04.064.

Keywords: Shear Deficient Beams, NSM, GFRP, Cyclic loading, Finite element, Nonlinear analysis, Reinforced concrete.

1.0 INTRODUCTION

Extensive research has been conducted recently to evaluate the response of externally bonded Fiber reinforced polymer (FRP) structural members including slabs, beams and columns [1-6]. FRP materials have high strength to weight ratio and anti-corrosion properties and considered to be the current most effective solutions in strengthening and repairing reinforced concrete (RC) structural members. Reinforced concrete beams are typically strengthened with externally bonded FRP sheets or laminates via epoxy adhesives. However, it was observed in many cases that debonding of the FRP materials from the concrete substrata occurs before achieving the theoretical full capacity of the strengthened member [7-8]. Debonding occurs when maximum shear stresses at the FRP level reaches its ultimate bond strength. Hence, success of a conventionally externally bonded FRP strengthening system is governed by the adhesion (bond) of the FRP and adjacent concrete surfaces. Furthermore, it should be noted that other factors might negatively influence the performance of externally strengthened systems such as temperature variations, freeze and thaw, and accidental impacts, among other factors.

FRP rods have been proposed as an alternative strengthening system to overcome some of the drawbacks of the externally bonded FRP plates and sheets. The FRP rods ~~are~~ will be attached to the structural member using the near surface mounting (NSM) technique. A typical NSM strengthening system consists of embedding FRP rods into precut grooves in the concrete cover. The grooves usually have square or rectangular cross sections and are usually filled with epoxy adhesives and/or high quality concrete. The major advantage of this strengthening system is that

the possibility of the debonding of FRP from the concrete substrate will be reduced. In addition, the quality of the concrete inside the groove is typically better than that of the surface concrete, in addition, NSM rods are protected by the concrete cover such that they will not be exposed to environment, and concrete surface preparation will no longer be needed. The contribution of carbon fiber polymer (CFRP) bars to the flexural capacity of RC beams was examined earlier [9-11]. However, little research has been conducted on the use of FRP rods for shear-dominant applications [12-14]. Those studies [12-14] showed that CFRP rods can provide significant increase in load carrying capacity for shear deficient beams. Furthermore, additional parameters such as the length of FRP rod, adhesive type, loading set-up, have been considered to study their influence in the overall behavior of NSM strengthened systems [15-16]. On the other hand, the use of GFRP reinforcements for shear strengthening has not been examined. This is mainly due to alkali silica reaction that prohibits the use of GFRP bars. However, test results confirmed that a properly designed and manufactured composite system of resin and glass can effectively protect the glass fibers from degradation. Therefore, there is a need to bridge the knowledge gap in this research area and to investigate the performance of RC beams strengthened with NSM GFRP bars.

Shear failure is brittle in nature and occurs without sufficient warning. Therefore strengthening structures deficient in shear is of great importance, especially in active seismic regions. Consequently, experimental investigation should be conducted to resemble seismic events by testing NSM GFRP strengthened RC beams subjected to cyclic loading. In addition, and to the best of the authors' knowledge, little research [17], if any has been published on finite element (FE) modeling of strengthened shear deficient RC beams with NSM GFRP bars under cyclic loading.

The aim of this study is to investigate experimentally and numerically the performance of RC beams externally strengthened in shear with NSM GFRP rods when subjected to cyclic loading. Five RC beams were experimentally tested under cyclic loading. In addition, five finite element (FE) models were developed to capture and validate the response of such strengthened structural members. The developed FE models were validated by comparing the load-deflection response envelopes and load-displacement hysteresis loops with that of the measured experimental data.

2.0 EXPERIMENTAL PROGRAM

2.1 Specimens Detailing and Material Properties

A total of five rectangular RC cantilever beams, 200 mm wide and 350 mm deep, were casted with a clear span of 1700 mm. The beams were designed to fail in shear without providing stirrups along the beams' span as shown in Fig. 1. Stirrups were only provided at the loading support to prevent local cracks that might occur due to applied load outside the shear span. The beams were attached to a rigid RC column to simulate the response of a fixed support. The column was heavily reinforced to prevent cracking and pre-mature failure. Figure 1 shows the geometrical details and the cross-sectional properties of the tested specimens and rigid RC column.

All beams were casted from the same batch of concrete with water, cement, sand and aggregate having a mass ratio of 0.68:1:2:3, respectively. Four cylinder specimens were casted and tested at the same time of beam test to determine the compressive strength of concrete. The measured average cylinder compressive strength after 28-days was approximately 25 MPa. The main longitudinal reinforcement consisted of eight 20 mm diameter deformed steel bars, four of which were located in the compression zone (top reinforcement) and the remaining four bars were

located in the tension zone (bottom reinforcement) of the members. A clear concrete cover of 30 mm was kept constant for all the tested specimens to overcome any possible embedding problems. The reinforcing bars used in the experimental program were tested in tension to obtain their mechanical properties. The measured yield strength of the longitudinal reinforcements was 414 MPa and 275 MPa, respectively.

The specimen designation and strengthening scheme detailing are listed in Table 1. BEAM-1 was used as a benchmark unstrengthened control specimen to establish a reference response. The remaining four shear deficient RC beams were strengthened with two legs of NSM GFRP bars located on both vertical sides of the beams' cross-section as shown in Fig. 2 with different GFRP bar diameters and spacing. Beam specimens BEAM-2 and BEAM-3 were strengthened with 6 mm diameter GFRP NSM rods spaced at 160, and 120 mm, respectively. On the other hand, BEAM-4, and BEAM-5 were strengthened with 10 mm diameter GFRP NSM rods spaced at 160, and 120 mm, respectively.

Uniaxial coupon tests were carried out in a servo-controlled test machine to obtain the mechanical properties of the GFRP bars including the stress-strain relationship, tensile strength and modulus of elasticity. The measured stress-strain relationships for the tested specimens were linear up to failure. The average obtained modulus of elasticity and tensile strength were found to be 40.6 GPa and 550 MPa, respectively. On the other hand, the epoxy adhesive used to bond the NSM GFRP bars to concrete surfaces had a tensile strength and secant tensile elastic modulus of epoxy as 30 and 3800, respectively.

BEAM-1 was used as a benchmark and tested without any additional FRP strengthening to establish a reference response. The remaining shear deficient RC beams were strengthened with GFRP bars with different diameters and spacing as shown in Table 1 . The parameters varied

herein were diameter of FRP rod as well as spacing used in between FRP reinforcement. Thus, specimens BEAM-2, and BEAM-3 were strengthened with 6 Ø diameter GFRP NSM rods spaced at 160, and 120 mm, respectively. On the other hand, BEAM-4, and BEAM-5 were strengthened with 10 Ø diameter GFRP NSM rods spaced at 160, and 120 mm, respectively.

2.2 Strengthening Procedure

Groove dimensions were cut depending on the bar diameter . The width of the groove is one and a half times the diameter of GFRP bar reinforcement. The vertical length of each groove was 350 mm, which is equal to the depth of the beam as shown in Fig. 2. The grooves were half-filled with the bonding epoxy adhesive. The GFRP reinforcement were subsequently inserted and lightly pressed to allow the adhesive to flow around the GFRP bar and avoid any pores between the bars and the sides of the groove. Afterwards, the grooves were filled with more epoxy adhesive and the surface was leveled by removing any additional epoxy. All applications were performed in a controlled lab environment at room temperature. The strengthened specimens were left to cure at room temperature for at least two weeks before testing.

2.3 Experimental Setup

A schematic view of the experimental set-up and arrangement of the measurement devices are depicted in Fig. 3. It is clear from Fig. 3 that the loading column has two hinges, a loading cell and a hydraulic jack. The capacity of the hydraulic jack and loading cell were 500 and 400 kN, respectively. Four linear variable differential transformers (LVDTs) were used to monitor displacements. The LVTD's are located at the end of the beam specimens for maximum vertical displacement under the rigid support to calculate the undesired displacement and finally on the rigid support to calculate the rotation. In addition, cycles of loading and unloading were applied at the free end of the cantilever beam. Load cycles were selected to evaluate flexural and shear cracks

propagations. Figure 4 shows a sample of the applied loading history. Loading was steadily increased up to yielding of the flexural top or bottom steel reinforcements or failure of the tested specimen.

3.0 EXPERIMENTAL RESULTS AND OBSERVATIONS:

The load-displacement hysteresis curves for the tested specimens measured at the free end of the cantilever beams are shown in Fig. 5. It should be noted that the first crack appeared as a flexural crack at a load between 33.18 kN and 39.65 kN for all the tested specimens, regardless of the strengthening scheme. As the load increment was increased, the initially developed flexural cracks were advanced through the member's sides and caused shear crack propagations. Similarly, shear cracks were also developed at the unstrengthened part of the specimen, between the GFRP bars. Thereafter, the behavior of the strengthened beams specimens showed deviation according to the strengthening scheme.

Figure. 6 draws a comparison between the load-deflection response envelope curves of the different specimens. The curves were plotted by connecting the peak loading values for each cycle versus their corresponding deflection values. It is clear from Fig. 6 that all the tested specimens have similar trend up to a load of about 30 kN. Afterwards, the behavior tends to deviate based on the strengthening scheme. Table 2 lists the ultimate attained load prior to failure along with the vertical deflection, and the increase in both the displacement and ultimate capacities compared to the unstrengthened specimen (BEAM-1).

It can be observed from Fig. 5, Fig. 6 and Table 2 that the use of the proposed NSM shear strengthening system with GRRP rods has significantly enhanced the cyclic load carrying

capacity of the tested specimens. The increase in load carrying capacity ranged between 49% and 66% of the control beam specimen (BEAM-1), depending on the rod diameter and rod spacing. In addition, the displacements at failure (ductility) of the strengthened specimens were more than that of the control unstrengthened specimen. The increase in the displacement over the control unstrengthened specimen ranged between 112% and 172%. Furthermore, the load carrying capacity has been slightly improved with increasing bar size from 6 mm to 10 mm and with reducing the spacing from 160 mm to 120 mm by less than 5.0%.

Three different failure mechanisms were observed in this experimental investigation. The observed failure mechanisms of the tested specimens were shear failure, shear failure due to concrete cover separation and flexural failure followed with shear failure. The control specimen, BEAM-1, failed in a shear mode due to the formation of a critical shear crack that was developed at a load of -61.90 kN as shown in Fig. 7.

BEAM-2 and BEAM-4 were strengthened with similar spaced GFRP bars at 160 mm (3/4d) center-to-center. The two specimens approximately depicted the same behavior where both failed due to concrete cover separation near the longitudinal tension reinforcement at the bottom of the beam as shown in Fig. 8. At 15 kN, flexural cracks appeared at the tension face. Then at approximately 35 kN, shear cracks occurred at the unstrengthened part between the GFRP rods. When the load exceeded 45 kN, shear cracks started to develop faster and wider and propagated to exhaust the body of the beam's web. This behavior continued until the load level reached 80 kN. BEAM-2, which was strengthened with 6 mm diameter GFRP bars, had sustained the 90 kN loading cycle but failed in the subsequent cycle at a load of 92.68 kN. BEAM-4 also sustained the forward loading of the 90kN cycle successfully and gained a slight

increase in strength due to larger-sized GFRP bar diameter. However the BEAM-4 specimen failed at a load level of 96.29 kN.

BEAM-3 and BEAM-5 were strengthened with 6 mm and 10 mm GFRP bars, respectively with 120 mm center-to-center (d/4) spacing. The behavior of both strengthened beams was similar up to a load level of 80 kN. Decreasing the spacing similar to BEAM-2 and BEAM-4 improved the behavior and the specimen at a load level of 98.11 kN. However, an abrupt shear failure occurred as shown in Fig. 7(c). It was expected that BEAM-5 would be able to achieve a better behavior and reach its flexural capacity. However, multiple cracks were visually observed in that cycle. In the next load cycle, BEAM-5 specimen exceed the 100 kN and the flexural steel reinforcement have yielded, larger cracks were observed when the load was 95 kN that led to flexural failure followed by a shear failure at a load level of 102.50 kN.

4. COMPUTATIONAL MODELING

4.1 Model Description

In previous studies [18-20], the authors developed finite element (FE) models that predicted the response of unstrengthened [18, 20] and also of externally strengthened [19] members under cyclic loading. One of the objectives of this study is to develop finite element models to numerically predict the performance of RC beams strengthened with NSM GFRP rods . In order to validate the results, the developed models have the same geometric and material properties of that of the five tested specimens presented in the preceding sections. Taking advantage of symmetry in geometry, loading and material properties in the beam's transverse direction, one-half 3D model were developed and cyclic loading was also applied

to the free end of the cantilever beams, and the analysis was performed using the FE software, ANSYS 11.0 [21]. Figure 10 shows a representative detailed sample of the developed model for a strengthened specimen with NSM GFRP rods.

The ANSYS SOLID65 [21] element was used to model the concrete and epoxy adhesives materials. The element has three degrees of freedom per node and is capable of simulating cracking in tension and crushing in compression. The column was heavily reinforced and didn't exhibit any cracking during loading. Thus, it was modeled with elastic material properties using SOLID45 element [21] which is very similar to SOLID65 but without the cracking or crushing capabilities. On the other hand, the steel and GFRP bars were modeled using LINK8 [21] element. The element is defined by two nodes that has three translational degrees of freedom per node and is capable of simulating elastic-plastic deformation.

ANSYS spring COMBIN14 [21] was used to simulate the bond-slip behavior between the GFRP rods and surrounding epoxy materials. The spring element is a uniaxial tension-compression element and is defined by its stiffness and has two nodes with up to three degrees of freedom per node. Determining the stiffness of the spring will be discussed in the subsequent section.

4.2 Material Properties

The mechanical material properties used as inputs in the developed FE model were similar to those used in measured the experimental program. Table 3 shows the mechanical material properties used in the FE simulation.

In order to numerically model the nonlinear behavior of concrete material, the concrete constitutive material model in ANSYS [21] is used. The concrete constitutive material model is based on the developed plastic model by William and Warnke [22]. William and Warnke model requires additional values for the open and closed shear coefficients that typically range from 0.0 and 1.0. In this study a value of 0.2 and 0.2 [18] was used for the open and closed shear coefficients, respectively. In addition, the constitutive material model for concrete in tension assumes concrete has a tri-linear behavior in tension. The tri-linear model starts with linear elastic segment up to the tensile strength of concrete (listed in Table 1). Once the concrete reaches its maximum tensile stress, a stiffness multiplier of 0.6 is used to simulate a softening in the tensile stress to 60% of the concrete maximum tensile stress f_t. In other words, in a given concrete element, once the maximum tensile strength is achieved, the cracked element experiences a sudden drop of strength equals to 0.6 f_t that represents the loss of stiffness induced by the cracks development. Further, this softening is followed by a linearly descending tensile response to zero stress at a strain equals to six times the maximum tensile strain. The nonlinear plastic behavior of concrete in compression is defined using the Hognestad parabola model [23].

The nonlinear response of the steel reinforcement bars is assumed to follow an elasto-plastic behavior. The modulus of elasticity and yield strength of the steel reinforcement are reported in Table 3. The Von-Misses failure criterion is used to define yielding of the steel

reinforcement. On the other hand, the GFRP rod NSM reinforcement was modeled as a brittle linear elastic material up to its tensile strength. The modulus of elasticity and tensile strength of the GFRP rods are shown in Table 3. Furthermore, the epoxy adhesive material was defined as an elastic material with the properties given in Table 3 up to its tensile strength. The epoxy material will crack and fails according to William and Wranke model, defined above, upon reaching its tensile strength. The elastic modulus and tensile strength of the epoxy material are also reported in Table 3.

The developed models take into account the bond-slip behavior between the bar reinforcement and surrounding material. The bond-slip action between the steel reinforcement and surrounding concrete material, as well as between the NSM GFRP rods and bonding material (epoxy) is simulated and it follows a set of relationships presented in CEB-FIP model [24]. The bond-slip relationship used in this study is described by Eq. 1.

$$\tau = \tau_u \left(\frac{s}{s_m} \right)^{0.4} \tag{1}$$

where,

τ is the bond stress at a given slip s (MPa),

τ_u is the maximum bond stress (MPa),

s is the relative slip at a given shear stress (mm),

s_m is the maximum slip at τ_m (mm),

Equation 1 follows the initial segment of CEB-FIP model [24]. The bond-slip behavior is used to calculate the stiffness of the spring COMBIN14 elements that follows the ascending segment of CEB-FIP model. Then, a horizontal plateau is set to equal the maximum bond stress

(τ_m) since the embedded reinforcement cannot completely debond from their substrates [25-27].

According to the CEB-FIB provisions, the value of the maximum bond stress depends on reinforcement bar type and adjoining material. According to the model [24], the values of $\sqrt{f_c'}$ and 0.6 mm were taken to simulate the values of τ_u and s_m respectively for the steel reinforcement. On the other hand, the values of τ_u and s_u of the GFRP rods were assumed based on the experimental programs of [28] to be 20.25 MPa, and 0.42 mm, respectively.

COMBIN14 elements require an input stiffness parameter (k) defined as the longitudinal stiffness. The longitudinal stiffness (k) of the spring element (COMBIN14) is calculated using Eq. 2 [29].

$$k = \frac{\pi}{s_u} p d_r N_r \tau_u \left(\frac{L_1 + L_2}{2} \right) \quad (2)$$

where,

p is the horizontal distance between the tension steel reinforcement bars in (mm), d_r is the diameter of the bars in (mm), N_r is the number of bars and L_1 and L_2 are the lengths of two adjacent bar elements in (mm). It should be noted that the adjacent nodes between the bars and epoxy or concrete materials are coupled in the transverse directions of the bar reinforcement.

4.3 Failure Criteria:

In general, failure in the FE simulation model is defined once divergence in the solution occurs. In this study, the force convergence criterion controls the convergence of Newton-Raphson solution scheme. After several trials, it was found that a convergence tolerance limit of 0.1 [17-19] led to convenient and optimum solution processing time. In addition, debonding

of the NSM GFRP rod from the epoxy (GFRP bar pull-out) was also considered as a failure criteria. The predicted ultimate load capacity of each beam specimen is defined when the solution for a 1 N load increment does not converge.

4.0 FINITE ELEMENT RESULTS AND VALIDATION

Five FE models were developed and have been numerically validated against the experimental data tested herein. The developed numerical models were distinguished using the prefix "FE" followed by the tested specimen designation BEAM-1, BEAM-2, BEAM-3, BEAM-4, and BEAM-5, respectively.

Figure 11 shows the predicted and measured load-deflection response envelope results of the tested specimens. The load-deflection response envelopes were developed by connecting peak edge deflection and loading values for the entire cyclic loading history.

Figure 12 displays the measured and the predicted load-deflection hysteresis curves. In addition, Table 4 shows a comparison between the predicted and the measured failure load and its corresponding deflection. It is clear from Figs. 11 and 12 and Table 4 that the developed FE model managed to successfully predict the response of the tested specimens at all stages of loading till failure of the specimens. Table 4 indicates that there is a good agreement between the tested and simulated FE numerical results with a maximum deviation less than 10%.

5.0 CONCLUSIONS

This paper presented an experimental and numerical simulation of shear deficient rectangular RC beams strengthened with NSM GFRP rods when subjected to cyclic loading. The following conclusions could be drawn from the outcomes of this research:

- Use of GFRP NSM strengthening system increased the overall capacity of the tested specimens and their ductility, regardless of the strengthening scheme.
- The use of the proposed NSM shear strengthening system with GRRP rods has significantly enhanced the cyclic load carrying capacity of the tested specimens. The increase in load carrying capacity ranged between 49% and 66% of the control beam specimen (BEAM-1), depending on the rod diameter and rod spacing.
- The use of the proposed NSM shear strengthening system with GRRP rods has also significantly enhanced the ductility of the beam by increasing the displacement. The displacements at failure (ductility) of the strengthened specimens were more than that of the control unstrengthened specimen and ranged between 112% and 172%.
- The load carrying capacity has been slightly improved when increasing the GFRP bar size from 6 mm to 10 mm and reducing the spacing from 160 mm to 120 mm. The improvement is less than 5.0%.
- The developed FE model in this study correlated, very well, the response of the tested specimens at all stages of the cyclic loading with a maximum deviation less than 10%.
- The developed model can be used as a valid tool for further future investigations of NSM GFRP strengthened RC beams in shear subjected cyclic loading using different schemes and configurations.

7.0 REFERENCES

[1] Guralnick S, Gunawan L. Strengthening of Reinforced Concrete Bridge Columns with FRP Wrap. Pract. Period. Struct. Des. Constr. 2006:11(4):218–228.

[2] Tanarslan M. Behavior of RC Beams Strengthened with Inclined CFRP Strips, Journal Of Reinforced Plastics And Composites 2010, DOI: 10.1177/0731684410371406

[3] El Maaddawy T, Soudki K, Strengthening of reinforced concrete slabs with mechanically-anchored unbonded FRP system, Construction and Building Materials 2008;22(4):444-455

[4] Kobayashi K. Innovative Application of FRPs for Seismic Strengthening of RC Shear Wall, ACI 2005:1269-1288

[5] Di Ludovico M, Prota A, Manfredi G, Cosenza E. FRP Strengthening of Full-Scale PC Girders, J. Compos. Constr. 2010;14:510

[6] Alsayed S, Al-Salloum Y, Almusallam T, Siddiqui N. Seismic Response of FRP-Upgraded Exterior RC Beam-Column Joints J. Compos. Constr. 2010;14: 95

[7] Smith S, Teng J. Shear-Bending Interaction in Debonding Failures of FRP-Plated RC Beams, Advances in Structural Engineering 2003;6(1):183-199

[8] Kotynia, R. Debonding Failures of RC Beams Strengthened With Externally Bonded Strips, Proceedings of the International Symposium on Bond Behaviour of FRP in Structures 2005:247-255

[9] El-Hacha R, Rizkalla S. Near-surface-mounted fiber-reinforced polymer reinforcements for flexural strengthening of concrete structures, ACI Struct J 2004;101(5):717–726.

[10] Barros J, Dias S, Lima J. Efficacy of CFRP-based techniques for the flexural and shear strengthening of concrete beams, Cement Concrete Compos 2007;29: 203–217.

[11] Triantafillou T, Antonopoulos C. Design of concrete flexural members strengthened in shear with FRP, J Compos Constr, ASCE 2000; 4(4):198–205.

[12] De Lorenzis L, Nanni A. Characterization of FRP rods as near-surface mounted reinforcement, J Compos Construc 2001; 5(2):114–121.

[13] Barros J, Sena-Cruz J, Dias S, Ferreira D, Fortes A. Near surface mounted CFRP-based technique for the strengthening of concrete structures. In: Workshop on R+D+I in technology of concrete structures—tribute to Dr. Ravindra Gettu, Barcelona, Spain, 2004. p. 205–17.

[14] Tanarslan M. The Effects of NSM CFRP Reinforcements for Improving the Shear Capacity of RC Beams, Construction and Building Materials 2011;25(5):2663-2673

[15] Anwarul Islam K, Effective methods of using CFRP bars in shear strengthening of concrete girders, Engineering Structures 2009;31(3):709-714

[16] Al-Mahmou F, Castel A, François R, Tourneur C. Strengthening of RC members with near-surface mounted CFRP rods, Composite Structures 2009; 91(2):138-147.

[17] Hawileh R, Tanarslan M, Naser M, and Abdalla JA. Experimental and Numerical Investigation on the Performance of Shear Deficient RC Beams Strengthened with NSM GFRP Reinforcement Under Cyclic Loading, 3rd ECCOMAS Thematic Conference on Computational Methods in Structural Dynamics and Earthquake Engineering, COMPDYN 2011, Corfu, Greece, 25–28 May 2011.

[18] Hawileh R, Abdalla JA, Tanarslan M. Modeling of Nonlinear Response of R/C Shear Deficient T-Beam Subjected to Cyclic Loading, Computers and Concrete 2012; 10(4): 413-428.

[19] Hawileh R, Abdalla JA, Tanarslan M, Naser M. Modeling of Nonlinear Cyclic Response of Shear-Deficient RC T-beams strengthened with Side Bonded CFRP Fabric Strips, Computers and Concrete 2011; 8(2): 193-206.

[20] Hawileh R, Rahman A, Tabatabai H. Nonlinear finite element analysis and modeling of a precast hybrid beam-column connection subjected to cyclic loads, Applied Mathematical Modelling 2010; 34(9): 2562-2583.

[21] ANSYS. Finite Element Computer Code. Version 11. ANSYS, Inc. Canonsburg, PA, 2007.

[22] William K, Warnke. Constitutive model for the triaxial behavior of, E., D. s.1.: In: Proceedings, international association for bridge and structural 1975, Vol. 19.

[23] Hognestad E, Hanson NW, McHenry D. Concrete stress distribution in ultimate strength design. ACI Journal 1955, Proceedings 52(12):455–479.

[24] Comite Euro-International du Beton (CEB-FIP). CEB-FIP model code 1990. Bulletin D'Information No. 213/214 (Concrete Structures), Lausanne, Switzerland; 1993.

[25] Hamid R, Crews K. Efficient finite element modelling of timber beams strengthened with bonded fibre reinforced polymers, Construction and Building Materials 2011; 25(8):3291-3300.

[26] De Lorenzis L, Scialpi V, La Tegola A. Analytical and experimental study on bonded-in CFRP bars in glulam timber, Compos Part B: Eng 2005;36(4):279–289.

[27] Hawileh R. Nonlinear finite element modeling of RC beams strengthened with NSM FRP Rods, Journal of Construction & Building Materials 2012; 27(1): 461-471.

[28] Lee J, Kim T, Kim T, Yi C, Park S, You Y, Park Y. Interfacial bond strength of glass fiber reinforced polymer bars in high-strength concrete, Composites Part B: Engineering 2008;39(2):258-270.

[29] Nie J, Fan J, Cai C. Stiffness and deflection of steel–concrete composite beams under negative bending. ASCE J Struct Eng. 2004;130(11).

Please cite this paper as:
G. Sakar, R.A. Hawileh, M.Z. Naser, J.A. Abdalla, M. Tanarslan, Nonlinear behavior of shear deficient RC beams strengthened with near surface mounted glass fiber reinforcement under cyclic loading, Materials & Design, Volume 61, September 2014, Pages 16-25, ISSN 0261-3069,
https://doi.org/10.1016/j.matdes.2014.04.064.

List of Figures:

Fig. 1. Detailing of Control Beam (BEAM-1)

Fig. 2. Strengthening Schemes of Strengthened Beam Specimens

Fig. 3. Schematic of test setup

Fig. 4. Cyclic applied load history

Fig. 5. Load-displacement hysteresis response curves for the tested specimens

Fig. 6. Load-deflection response envelope curves of the tested specimens

Fig.7.Failure of control specimen

Fig. 8. Failure mode, Beam 2 and Beam 4

Fig. 9. Sample of the failure Modes observed in the experimental program

Fig. 10. Details of the developed FE model

Fig. 11. Predicted and measured load-deflection response envelope results

Fig. 12. Measured and Predicted load-deflection hysteresis curves

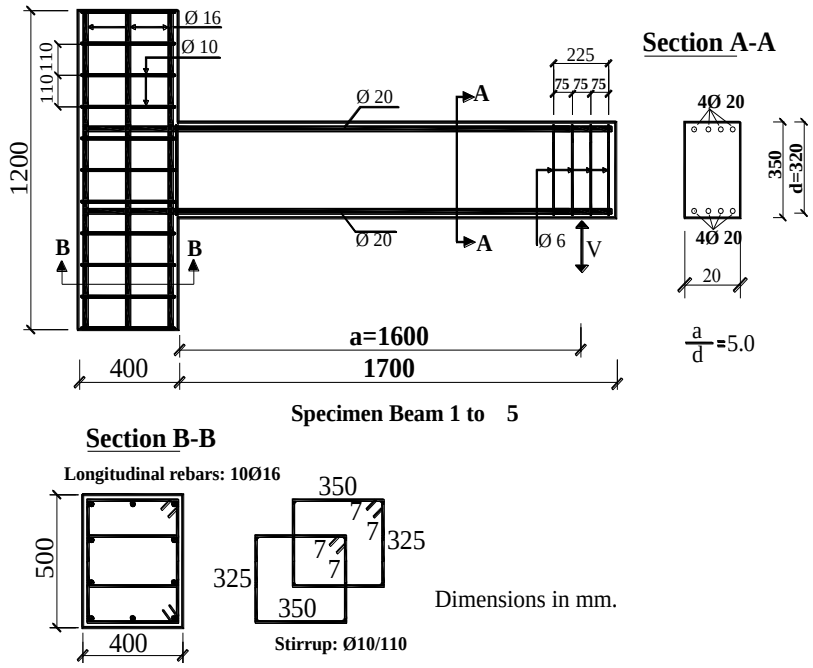

Fig. 1. Detailing of Control Beam (BEAM-1)

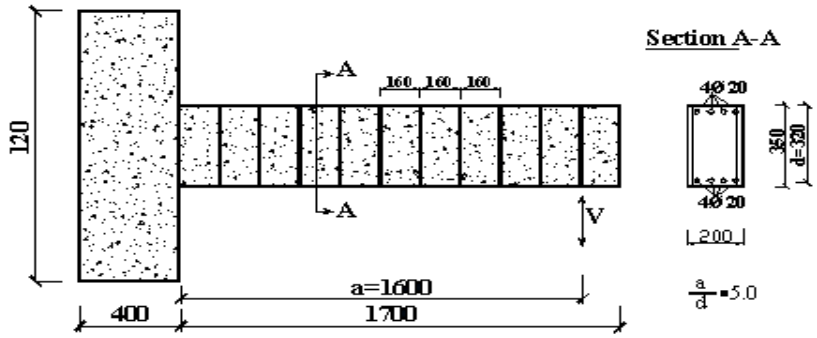

(a) BEAM-2 and BEAM-4

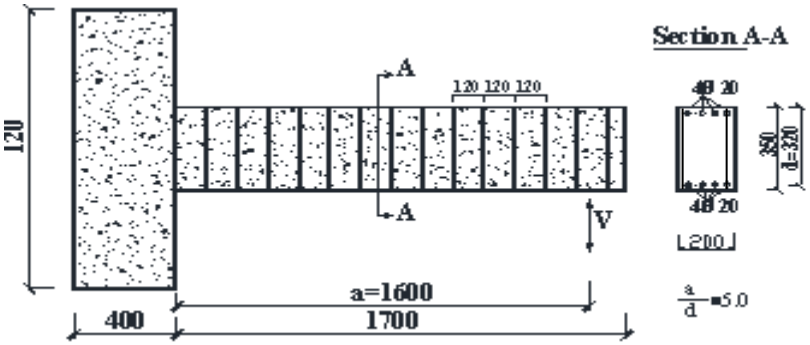

(b) BEAM-3 and BEAM-5

Fig. 2. Strengthening Schemes of Strengthened Beam Specimens

Please cite this paper as:
G. Sakar, R.A. Hawileh, M.Z. Naser, J.A. Abdalla, M. Tanarslan, Nonlinear behavior of shear deficient RC beams strengthened with near surface mounted glass fiber reinforcement under cyclic loading, Materials & Design, Volume 61, September 2014, Pages 16-25, ISSN 0261-3069,
https://doi.org/10.1016/j.matdes.2014.04.064.

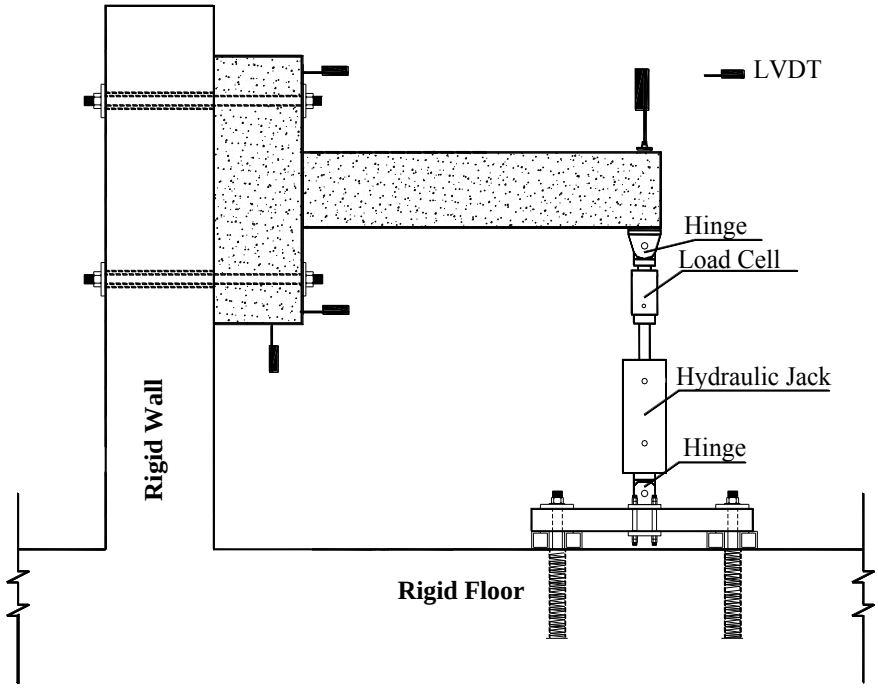

Fig. 3. Schematic of test setup

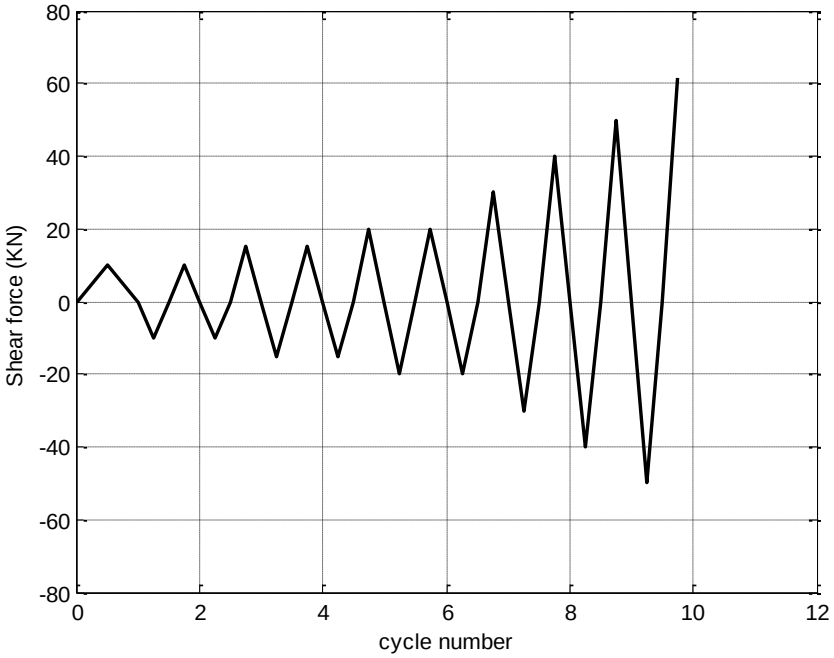

Fig. 4. Cyclic applied load history

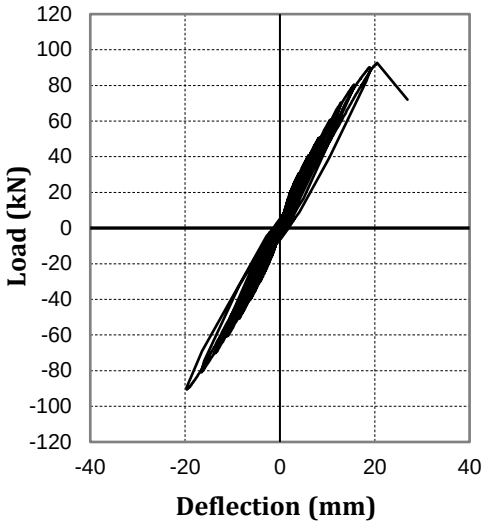

BEAM-1

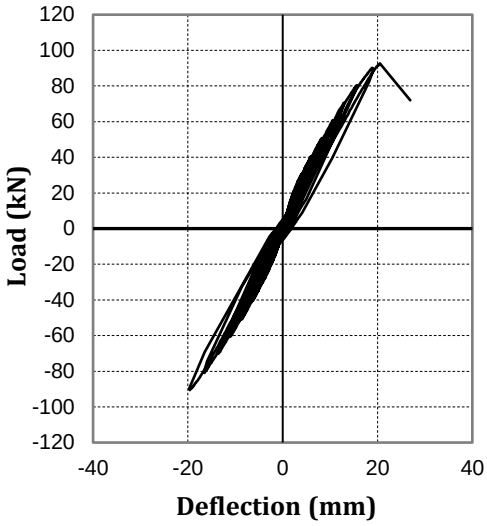

BEAM-2

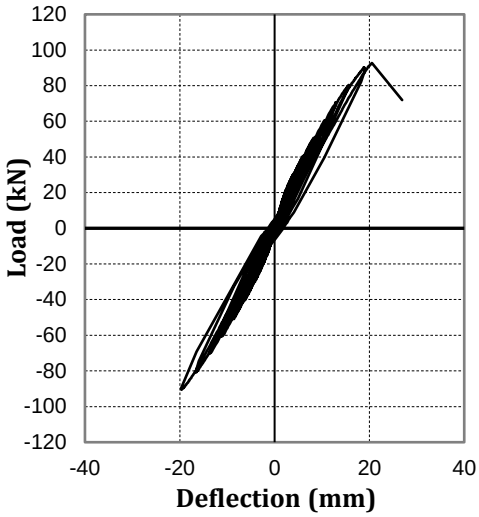

BEAM-3

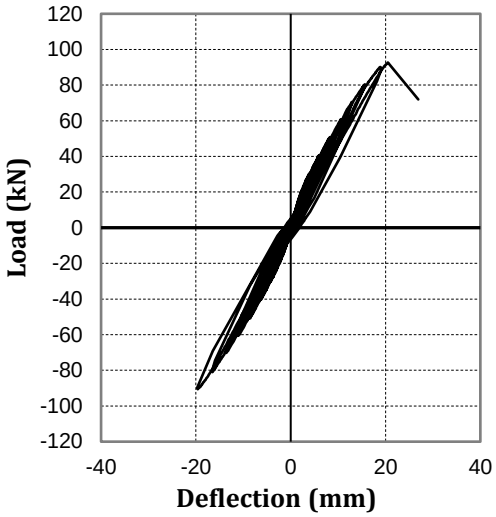

BEAM-4

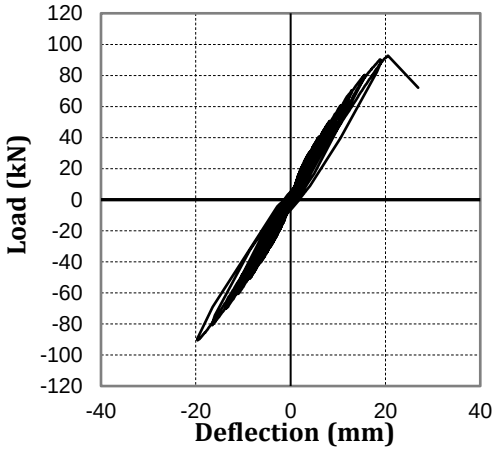

BEAM-5

Please cite this paper as:
G. Sakar, R.A. Hawileh, M.Z. Naser, J.A. Abdalla, M. Tanarslan, Nonlinear behavior of shear deficient RC beams strengthened with near surface mounted glass fiber reinforcement under cyclic loading, Materials & Design, Volume 61, September 2014, Pages 16-25, ISSN 0261-3069,
https://doi.org/10.1016/j.matdes.2014.04.064.

Fig. 5. Load-displacement hysteresis response curves for the tested specimens

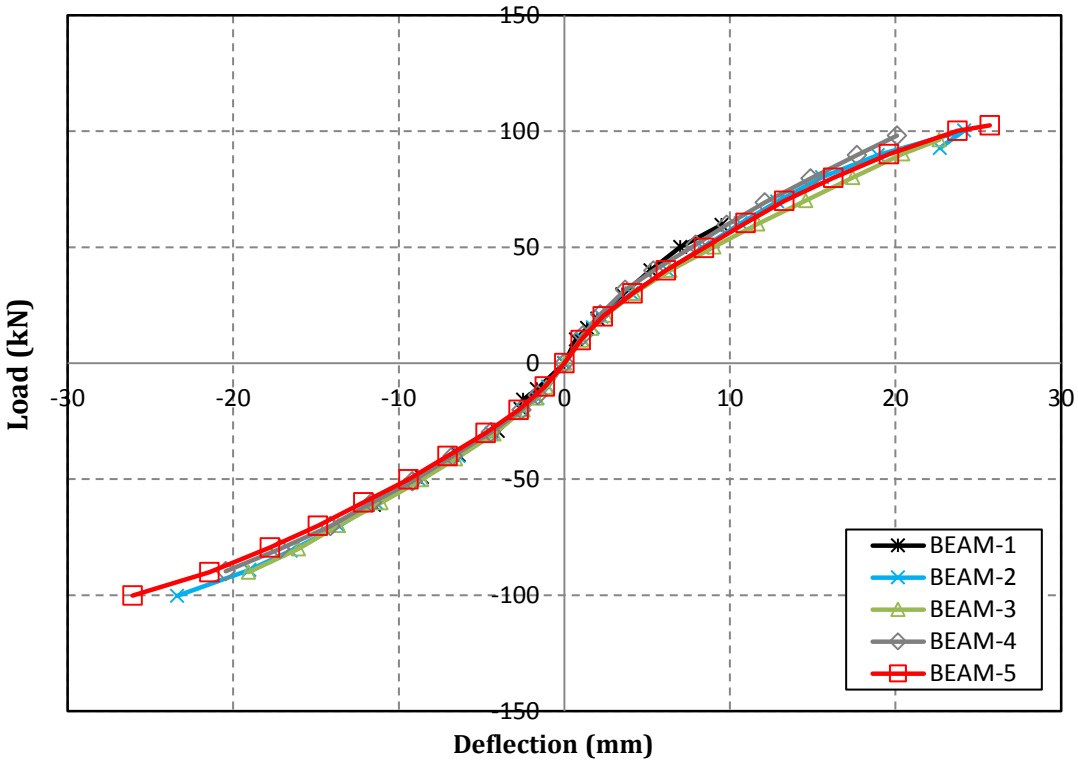

Fig. 6. Load-deflection response envelope curves of the tested specimens

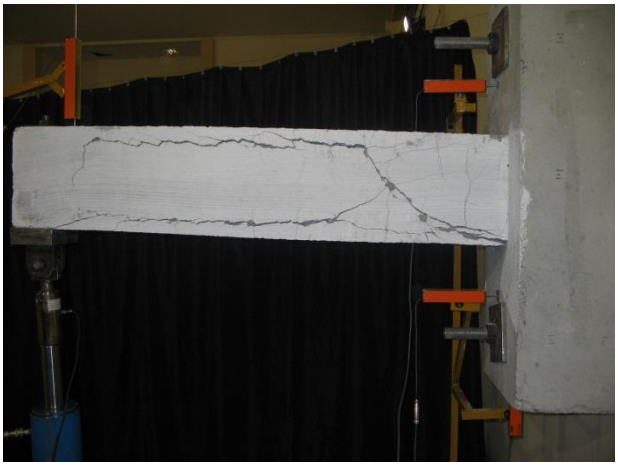

Fig.7.Failure of control specimen

Fig. 8. Failure mode, Beam 2 and Beam 4

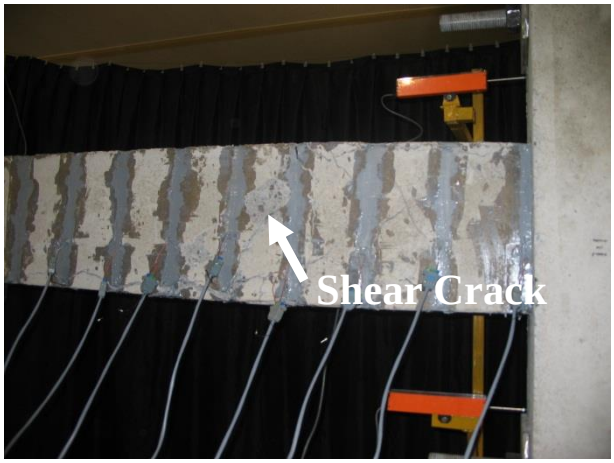

Fig. 9. Sample of the failure Modes observed in the experimental program

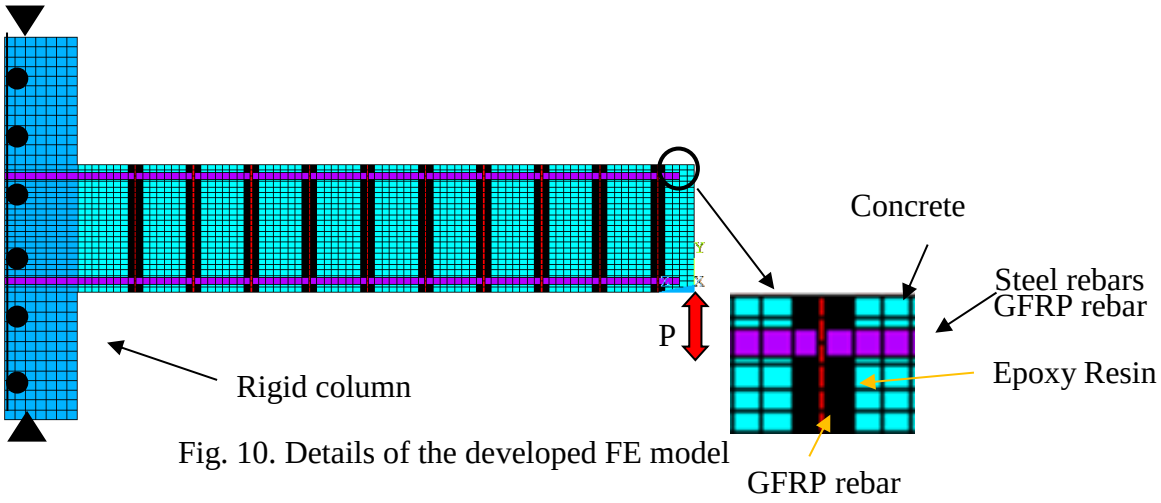

Fig. 10. Details of the developed FE model

Please cite this paper as:
G. Sakar, R.A. Hawileh, M.Z. Naser, J.A. Abdalla, M. Tanarslan, Nonlinear behavior of shear deficient RC beams strengthened with near surface mounted glass fiber reinforcement under cyclic loading, Materials & Design, Volume 61, September 2014, Pages 16-25, ISSN 0261-3069,
https://doi.org/10.1016/j.matdes.2014.04.064.

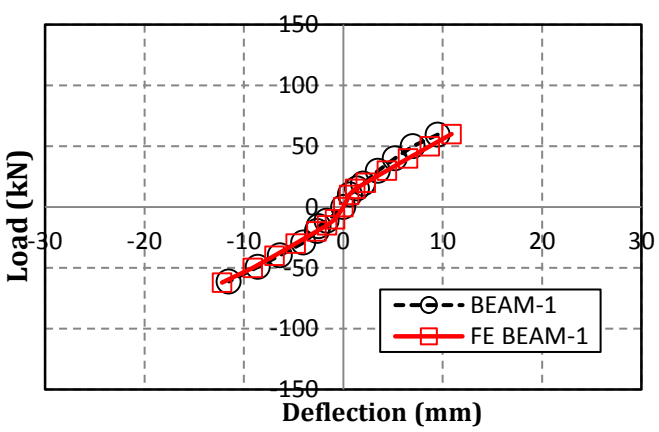

BEAM-1

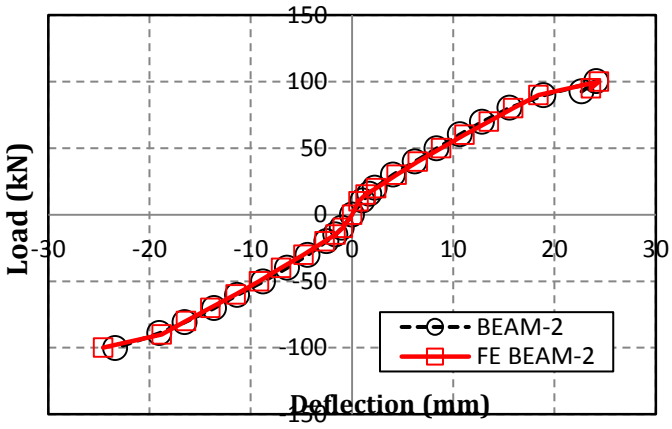

BEAM-2

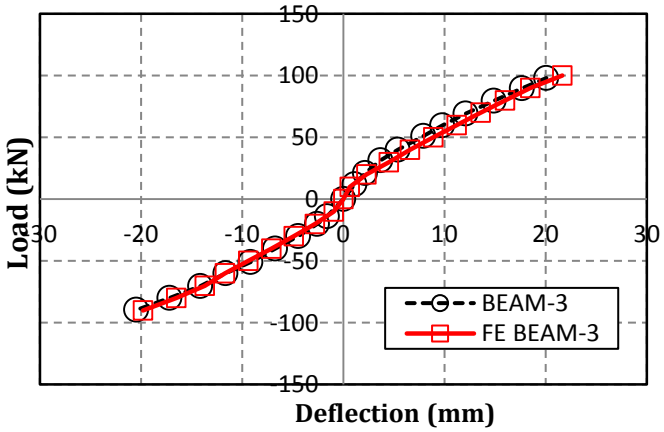

BEAM-3

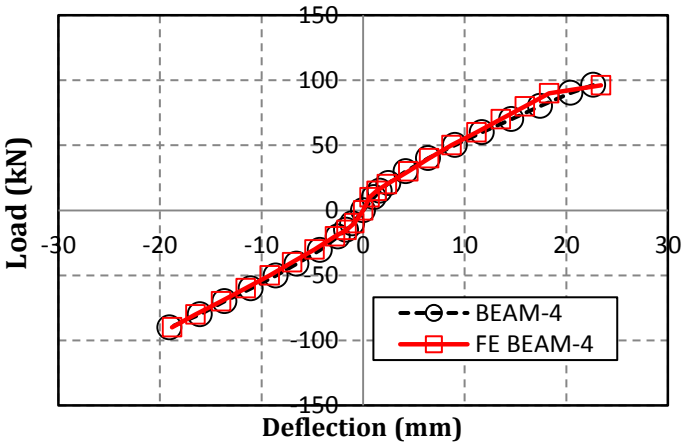

BEAM-4

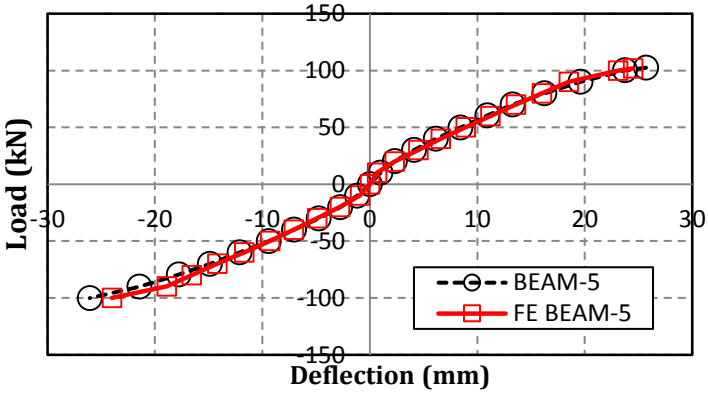

BEAM-5

Fig. 11. Predicted and measured load-deflection response envelope results

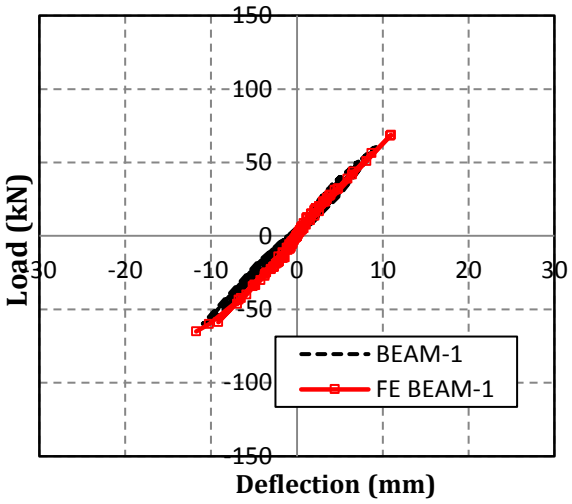

BEAM-1

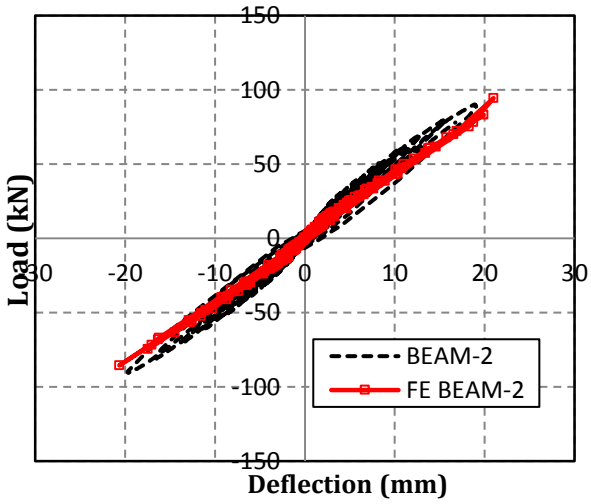

BEAM-2

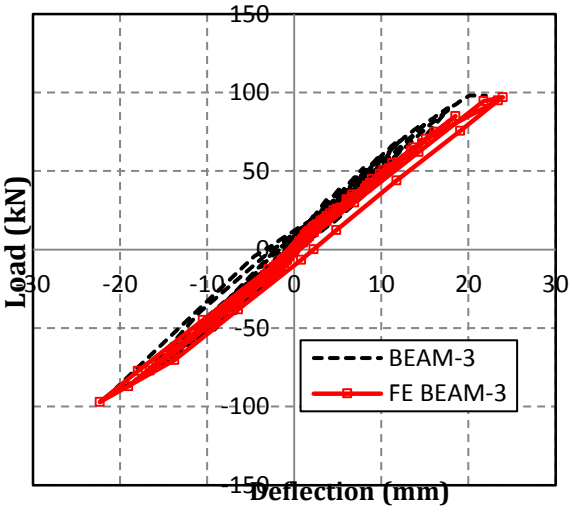

BEAM-3

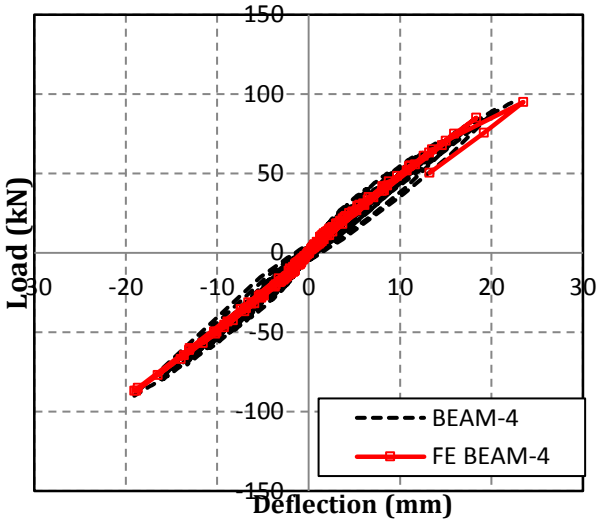

BEAM-4

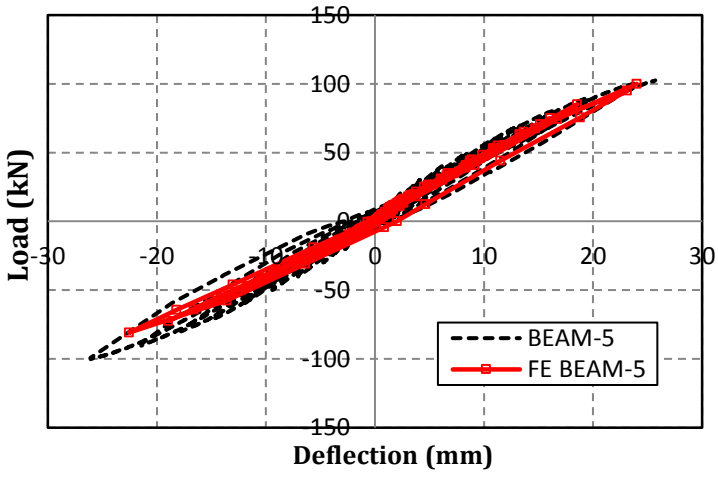

BEAM-5

Fig. 12. Measured and Predicted load-deflection hysteresis curves

List of Tables:

Table 1 Properties of tested specimens

Table 2 Measured experimental results

Table 3 Material Properties used in the FE simulation

Table 4 Comparison between the FE predicted and experimental measured results

Table 1 Properties of tested specimens

Specimen		NSM GFRP Reinforcement Details		
		Diameter (mm)	Spacing (mm)	Arrangements
BEAM-1	(Control)	------	------	------
BEAM-2	(Strengthend)	6 Ø	160	Both side
BEAM-3	(Strengthend)	6 Ø	120	Both side
BEAM-4	(Strengthend)	10 Ø	160	Both side
BEAM-5	(Strengthend)	10 Ø	120	Both side

Table 2 Measured experimental results

Specimen	Ultimate Load (kN)	Ratio Load increase to BEAM-1	Failure Displacement (mm)	Ratio Displacement increase to BEAM-1
BEAM-1	-61.90	-	9.46	-
BEAM-2	92.68	1.49	22.68	2.40
BEAM-3	98.11	1.58	20.08	2.12
BEAM-4	96.29	1.56	22.64	2.39
BEAM-5	102.50	1.66	25.70	2.72

Please cite this paper as:
G. Sakar, R.A. Hawileh, M.Z. Naser, J.A. Abdalla, M. Tanarslan, Nonlinear behavior of shear deficient RC beams strengthened with near surface mounted glass fiber reinforcement under cyclic loading, Materials & Design, Volume 61, September 2014, Pages 16-25, ISSN 0261-3069,
https://doi.org/10.1016/j.matdes.2014.04.064.

Table 3 Material Properties used in the FE simulation

Material	Compressive strength (MPa)	Yield strength (MPa)	Tensile strength (MPa)	Elastic Modulus (GPa)	Poisson ratio
Concrete	25.0	-	3.1*	24.0**	0.20
Steel	-	414.0	-	200.0	0.30
GFRP	-	-	550.0	40.8	0.28
Epoxy	-	-	30.0	3.80	0.29

* $f_t = 0.62\sqrt{f_c'}$ in MPa

** $E_x = 4800\sqrt{f_c'}$ in MPa

Table 4 Comparison between the FE predicted and experimental measured results

Specimen	**FE Model**	**Failure Load (kN)**		**Percentage Difference**	**Maximum Deflection (mm)**		**Percentage Difference**
		Exp.	FE	(FE/Exp.)	Exp.	FE	(FE/Exp.)
BEAM-1	FE BEAM-1	-61.90	-62.1	0.32%	-11.69	-12.2	4.3%
BEAM-2	FE BEAM-2	92.68	95.05	2.55%	20.68	21.6	1.04%
BEAM-3	FE BEAM-3	98.11	100.0	1.92%	20.08	21.67	7.90%
BEAM-4	FE BEAM-4	96.29	96.0	-0.30%	22.64	23.4	3.35%
BEAM-5	FE BEAM-5	102.50	103.0	0.49%	25.70	24.5	-4.67%